Electronic Supplementary Material (ESI) for Physical Chemistry Chemical Physics


# Electronic Supplementary Information for: A Mechanistic Study of the Electrochemical Oxygen Reduction on the Model Semiconductor n-Ge(100) by ATR-IR and DFT

Simantini Nayak, P. Ulrich Biedermann, Martin Stratmann, Andreas Erbe

## 1 Experimental vibrational frequencies of reference compounds

### 1.1 Oxygen-containing species

#### 1.1.1 Raman spectra of $KO_2$ and $O_2$

Stable superoxides can be used to check the vibrational frequencies obtained from DFT calculations. To that end, the Raman spectrum of $KO_2$ powder (ABCR, Karlsruhe, Germany) on a Si wafer was recorded using a Horiba Labram 2 confocal Raman microscope with 633 nm excitation. The spectrum is shown in Figure 1a, with peak maximum at 1145 $cm^{-1}$.

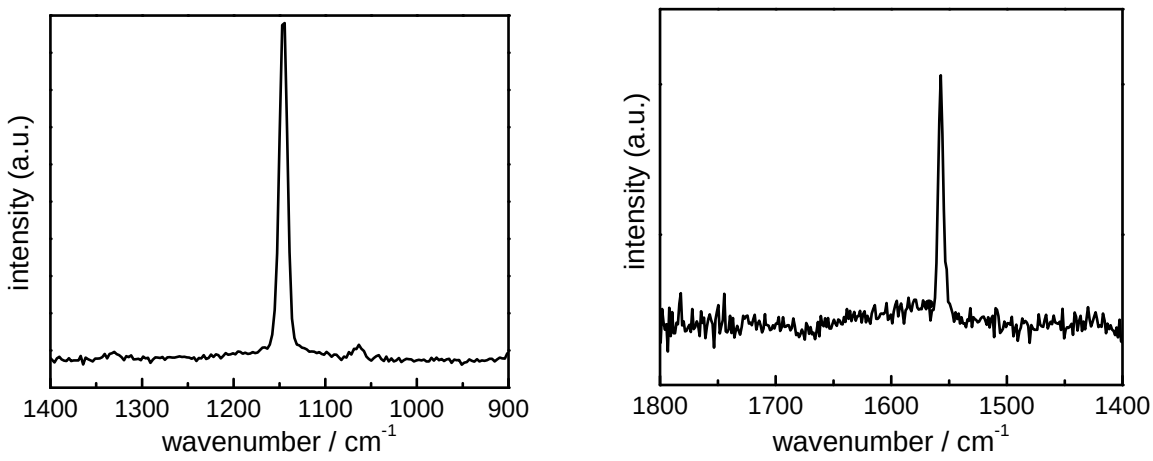


(a) (b)

Figure 1: (a) Raman spectrum of solid $KO_2$. (b) Raman spectrum of air.

A Raman spectrum of air was recorded using the Horiba Labram 2 confocal Raman microscope, but this time with 514 nm excitation at full power of the $Ar^+$ laser. The spectrum is shown in Figure 1b, with a peak maximum at (1558±1) $cm^{-1}$.

### 1.1.2 IR ellipsometry of $H_2O_2$ solution

To obtain reliable information about the vibrational modes from $H_2O_2$ and $OOH^-$, IR reflection ellipsometry measurements at the air/water interface have been carried out using a Sentech Sendira IR spectroscopic ellipsometer, equipped with DTGS detector, at a Biorad FTS 3000 FTIR spectrometer. A reflection experiment was chosen due to the corrosive nature of alkaline $H_2O_2$ towards transmission and ATR cell materials. Using the equation for the pseudodielectric function (eq. 3.58 in [1]), the absorption coefficient (*i.e.*, imaginary part of the refractive index) has been obtained for concentrated (30 %) aqueous $H_2O_2$ solution at pH 6.5, and a saturated solution of NaOH in 30 % aqueous $H_2O_2$.

Results are presented in Figure 2. The spectra are dominated by the vibrational modes of water. In $H_2O_2$, a broad peak is visible centered at 1380 $cm^{-1}$. Upon deprotonation of $H_2O_2$, a peak at 1310 $cm^{-1}$ appears, while no other absorption peak is visible between 900 and 1300 $cm^{-1}$.

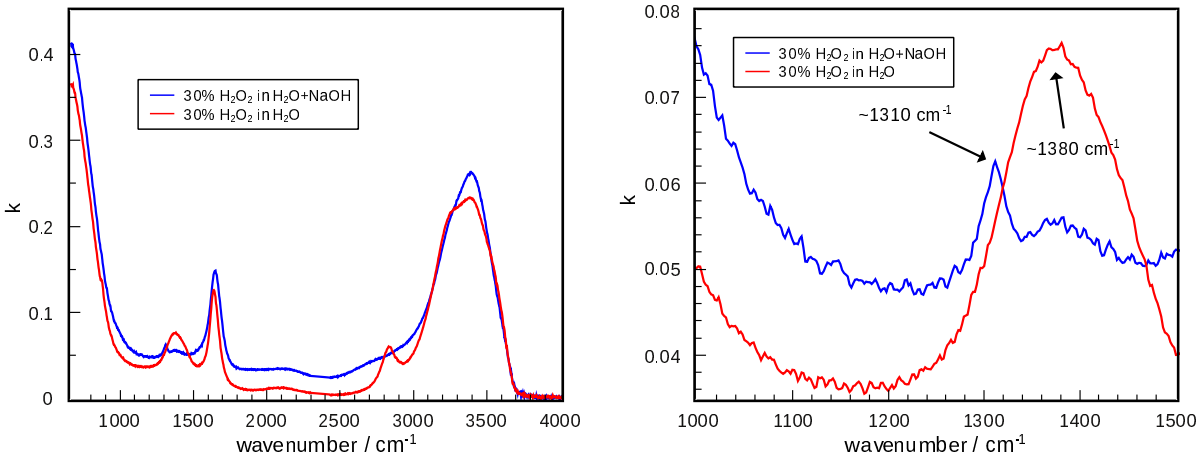


Figure 2: Imaginary part $k$ of refractive index for concentrated aqueous $H_2O_2$ solution (—) and alkaline $H_2O_2$ solution (—). (a) Full spectra. (b) Region 1000 $cm^{-1}$ – 2000 $cm^{-1}$.

## 1.2 Perchlorate-related species

For reference, the ATR-IR spectrum of the bulk electrolyte in the spectral region of interest is given in Figure 3. This spectrum was obtained using the same setup as used to record the spectra presented in the main article, at open circuit, using air as background and the electrolyte as sample spectrum. The slope of the baseline is due to the beginning absorption from librational modes of water. The spectrum shows only one single broad peak between 1000 and 1400 $cm^{-1}$, which is centered at 1105 $cm^{-1}$. Here, no peak is visible around 1030 $cm^{-1}$.

## 1.3 Literature survey of vibrational frequencies and assignments of ORR intermediates

Table 1 gives an overview over reported assignments of IR and Raman frequencies for oxygen-related species reported in the literature from other spectroelectrochemical experiments. For comparison, spectral data for selected stable reference compounds is also included. In addition, electrolyte species relevant for this work are also included.

| wavenumb. | species | mode | sample / substrate | technique | ref. |
|---|---|---|---|---|---|
| 697 | $O_2^{2-}$ | $\nu$(O–O) | Ag film | SERS | [2] |
| 815-830 | M-OOH | $\nu$(O–O) | Au | SERS | [3] |
| 864 | $H_2O_2$ | $\nu$(O–O) | vapour | Raman | [4] |
| 1005-1016 | $O_2^{\bullet-}$ | $\nu$(O–O) | rough Pt film | ATR-SEIRAS | [5] |
| 1105 | $ClO_4^-$ | $\nu_{as}(ClO_4)$ | 0.1 M $HClO_4$ * | ATR-IR | this work |
| 934, 1113 | $ClO_4^-$ | $\nu_s$, $\nu_{as}(ClO_4)$ | dilute $HClO_4$ * | Raman | [6] |
| 1039, 1220 | $HClO_4$ | $\nu_s$, $\nu_{as}(ClO_3)$ | $HClO_4$ * | Raman | [6] |
| 1047, 1080 | $O_2^{\bullet-}$ | $\nu$(O–O) | rough Au film | SERS | [7] |
| 1053 | $O_2^{\bullet-}$ | $\nu$(O–O) | Ag film | SERS | [2] |
| 1090 ± 20 | $O_2^{\bullet-}$ | $\nu$(O–O) | He gas discharge | UV-PES | [8] |
| 1125 | $HO_2^{\bullet}$ | $\nu$(O–O) | vacuum | UV-PES | [9] |
| 1132 | $O_2^{\bullet-}$ | $\nu$(O–O) | $CsO_2$ * | reson. Raman | [10] |
| 1143 | $O_2^{\bullet-}$ | $\nu$(O–O) | $KO_2$ * | reson. Raman | [10] |
| 1145 | $O_2^{\bullet-}$ | $\nu$(O–O) | $KO_2$ * | Raman | this work |
| 1150 | $O_2^{\bullet-}$ | $\nu$(O–O) | rough Au film | SERS | [11] |
| 1165 | $HO_2^{\bullet}$ | $\nu$(O–O) | rough Au film | SERS | [12] |
| 1250 | $O_2^{\bullet-}$ | $\nu$(O–O) | Au foil | IRRAS | [13] |
| 1268 | $HO_2^-$ | $\delta$(O–O–H) | rough Au film | ATR-SEIRAS | [14] |
| 1310 | $HO_2^-$ | $\delta$(O–O–H) | 30% $H_2O_2$ + NaOH * | IR ellipsometry | this work |
| 1390 | $H_2O_2$ | $\delta$(O–O–H) | 30% $H_2O_2$ * | IR ellipsometry | this work |
| 1394 | $H_2O_2$ | $\delta$(O–O–H) | $H_2O_2$ vapour * | Raman | [4] |
| 1400-1403 | $O_2$ | $\nu$(O–O) | Pt particles / Nafion | FTIR | [15] |
| 1550 | $O_2$ | $\nu$(O–O) | rough Bi/Au film | SERS | [12] |
| 1556 | $O_2$ | $\nu$(O–O) | $O_2$ (gas) * | Raman | [16] |
| 1558 | $O_2$ | $\nu$(O–O) | air (gas) * | Raman | this work |

Table 1: Comparison of experimental frequencies, in $cm^{-1}$, reported for intermediates during ORR and of selected reference compounds. The reference compounds are labelled by *. Abbreviations: IRRAS: IR reflectance absorption, SEIRAS: surface enhanced IR absorption spectroscopy, SERS: surface enhanced Raman scattering, UV-PES: ultraviolet photoelectron spectroscopy.

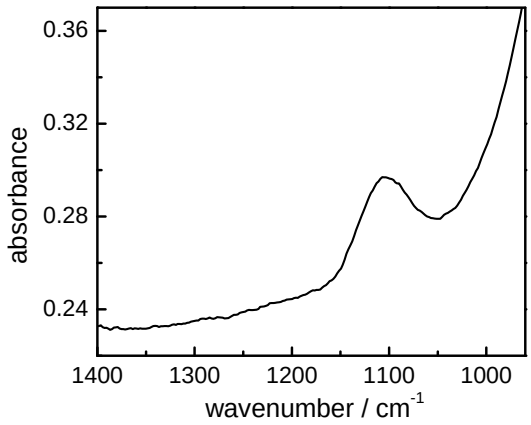


Figure 3: ATR-IR spectrum of 0.1 M $HClO_4$ in contact with n-Ge(100) crystal.

A linear dependece of the O–O stretching frequency on the redox state of dioxygen species has been noted in the Literature [2, 17]. On the other hand, the frequencies reported for $\nu$(O–O) of the superoxide anion radical, $O_2^{\bullet -}$, adsorbed on various metal surfaces show a very wide spread (1005-1250 $cm^{-1}$). This could be due to possible ambiguities in the identification of the species and mode or to a very strong effect of metal adsorption on this vibrational frequency. The same situation applies to the frequencies reported for $\nu$(O–O) of $HO_2^{\bullet}$ (1125 or 1165 $cm^{-1}$), for $\delta$(O–O–H) of $HO_2^-$ (1268 or 1310 $cm^{-1}$) and for $\nu$(O–O) of molecular oxygen ($\sim$1400, 1500 or 1556 $cm^{-1}$) in different environments (Table 1). Due to the possible ambiguities in experimental assignments and the large variations in the observed O–O stretching frequencies for each of the species, we used DFT calculations to identify the species corresponding to ORR-related IR absorptions observed here.

## 1.4 Survey of surface-bound species

For the purpose of an extensive search for Ge-bound species that give rise to vibrational frequencies in the range of 1000 - 1400 $cm^{-1}$ a fairly small and simple model was selected and solvation effects were neglected in the first approximation. After the identification of candidate structures for the experimental observations, larger models including solvation are used to arrive at better estimates for the vibrational frequencies. Initially, the Ge(100) surface is represented by a cluster of 3 Ge atoms with the general structure $(H_3Ge)_2GeXY$, where the central Ge represents the surface atom bound to two sub-surface Ge atoms with H-atoms saturating their dangling bonds. The subsituents X and Y may represent different surface terminations or functional groups related to the ORR. The structures considered are shown in Figure 4 and the vibrational frequencies due to the substituents are summarized in Table 2. In each case, only the lowest energy conformation is presented.

| species | | wavenumbers | | | | |
|---|---|---|---|---|---|---|
| | | $\nu$(O–H) | $\nu$(Ge–H) | $\delta$(O–O–H) | $\nu$(O–O) | $\nu$(Ge–O) |
| $(H_3Ge)_2GeH_2$ | (a) | | 2039/2030 | | | |
| $(H_3Ge)_2Ge(H)$–OH | (b) | 3707 | 1987 | 894 | | 633 |
| $(H_3Ge)_2Ge(OH)_2$ | (c) | 3695/3694 | | 875/874 | | 644/636 |
| $(H_3Ge)_2Ge{=}O$ | (d) | | | | | 916 |
| $(H_3Ge)_2Ge^{\bullet}(–H)$ | (e) | | 1981 | | | |
| $(H_3Ge)_2Ge^{\bullet}(–OH)$ | (f) | 3698 | | 859 | | 627 |
| $(H_3Ge)_2Ge(H)$-$O^{\bullet}$ | (g) | | 1992 | | | 608 |
| $(H_3Ge)_2Ge(H)$-OOH | (h) | 3630 | 2001 | 1294 | 886 | 592 |
| $(H_3Ge)_2Ge{<}O_2$ | (i) | | | | 849 | 610/558 |
| $((H_3Ge)_2Ge(H)–O)_2$ | (j) | | 2032/2031 | | 952 | 597/442 |
| $(H_3Ge)_2Ge(H){<}O_2^-$ | (k) | | 1927 | | 816 | 593/388 |
| $(H_3Ge)_2Ge(H)–OO^{\bullet}$ | (l) | | 2025 | | 1126 | 533 |
| $(H_3Ge)_2Ge(H)–O–ClO_3$ | (m) | | 2047 | 1218/1178/992 [a] | | 636 |

[a]: $\nu$(Cl–O)

Table 2: Selected vibrational frequencies of Ge(100) surface-bound species, in $cm^{-1}$ calculated with B3-LYP/def2-TZVP. The second column gives the part of Figure 4 which contains the geometry-optimized version of the structure.

The structures shown in the first row of Figure 4(a-d) correspond to a fully reduced (Figure 4a), partly reduced (Figure 4b) and fully oxidized surface (4c,d). The second row (Figure 4e-g) includes surface radicals, which are possible reactive intermediates in the change of surface termination. The last two rows (Figure 4h-m) show possible intermediates due to the ORR (Figure 4h-l) and a surface-bound perchlorate (Figure 4m).

The surface-bound peroxide $(H_3Ge)_2Ge(H)$–OOH (Figure 4h) has a $\delta$(O–O–H) bending mode at 1294 $cm^{-1}$, which is close to that of $H_2O_2$ in the gas phase and identified as a candidate structural motif for the 1385 $cm^{-1}$ IR absorption observed during ORR. The peroxo species bridging two surface Ge-atoms, $((H_3Ge)_2Ge(H)\text{-}O)_2$ (Figure 4j), has a vibrational mode at the lower limit of the range of interest. Calcuations of larger models that better represent the distances and bond angles at the Ge(100) surface indicated a shift to lower frequencies (not shown). Therefore this structural motif was excluded from further investigations. The surface-bound superoxide $(H_3Ge)_2Ge(H)$-$OO^{\bullet}$ (Figure 4l) has a $\nu$(O–O) stretching mode at 1126 $cm^{-1}$, which is close to those of $HOO^{\bullet}$ and $O_2^{\bullet-}$ and is identified as a candidate structural motif for the 1210 $cm^{-1}$ IR absorption observed during ORR. The other possible ORR intermediates show vibrational frequencies outside the range of interest in this study, and are therefore not discussed any further.

Finally, the perchlorate-bound via one O-atom to the surface, $(H_3Ge)_2Ge(H)$–O–$ClO_3$ (Figure 4m) has a symmetric $\nu$(Cl–O) stretching mode at 992 $cm^{-1}$, reasonably close to the 1030 $cm^{-1}$ IR absorption observed during ORR. Furthermore the asymmetric $\nu$(Cl–O) stretching modes at 1218 and 1178 $cm^{-1}$ are also in the range of interest.

Thus, several structural motifs have been found that give rise to vibrational frequencies in the range of interest, reasonably close to the IR features observed during ORR. However, it should be noted that the corresponding TDMs are less upright than those observed in the experiments. Actually, the surface-bound superoxide $(H_3Ge)_2Ge(H)$–$OO^{\bullet}$ has a downward tilting conformation, which is impossible on a flat surface due to steric repulsion. The above calculations for the interesting structural motifs have to be refined using a larger Ge-cluster capable of representing the excluded volume due to neighboring $GeH_2$ surface groups on the

Ge(100) surface. Furthermore, solvent effects should be included.

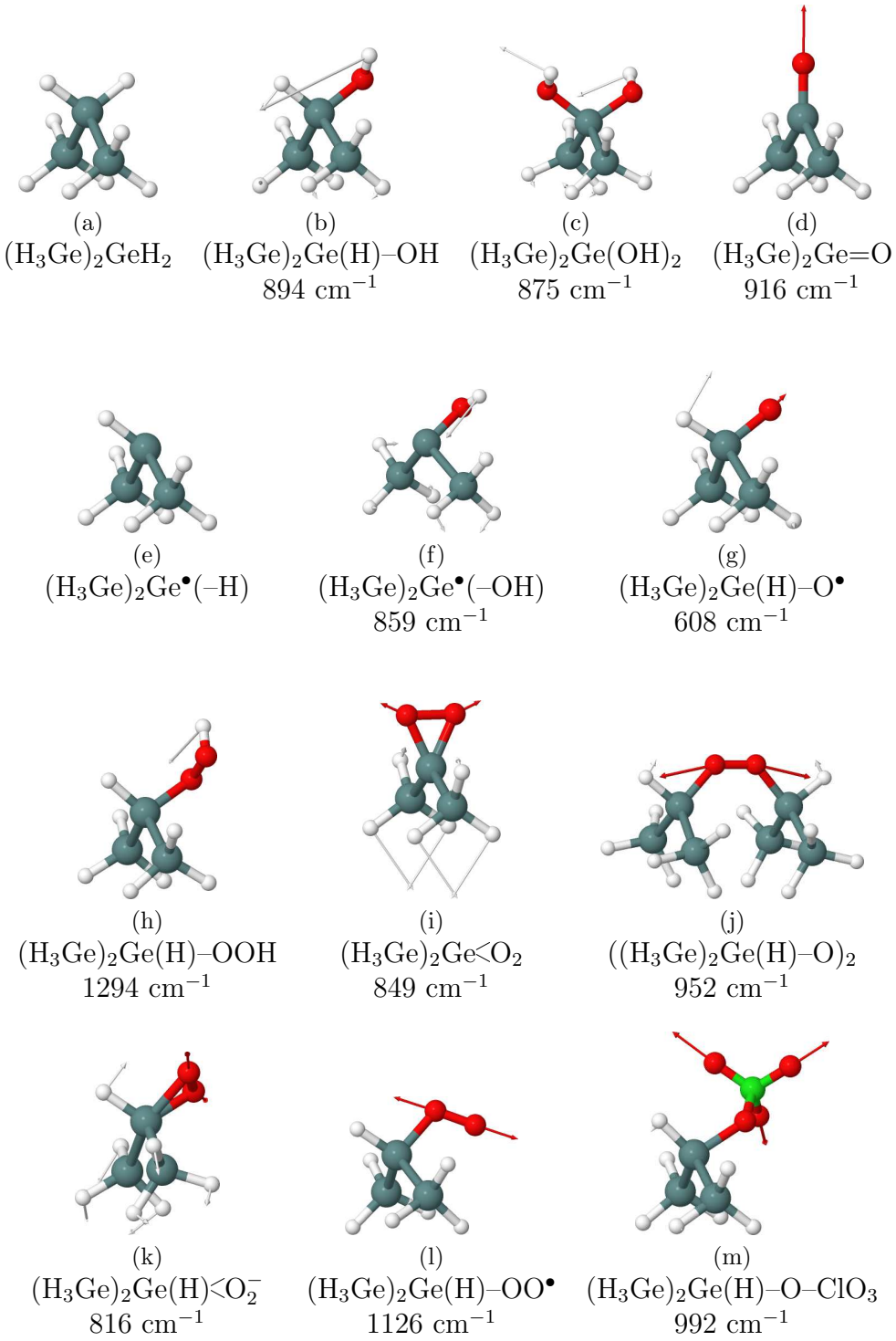


Figure 4: Structures of the $(H_3Ge)_2GeXY$ surface clusters calculated with B3-LYP/def2-TZVP. Important vibrational modes are shown by arrows indicating the motions of the atoms with the respective color. An overview over the relevant frequencies is given in Table 2.

# References

[1] J. Gerald E. Jellison, in *Handbook of Ellipsometry*, ed. H. G. Tompkins and E. A. Irene, Springer, Heidelberg, 2005, ch. 3. Data Analysis for Spectroscopic Ellipsometry, pp. 237–296.

[2] C. Pettenkofer, I. Pockrand and A. Otto, *Surf. Sci.*, 1983, **135**, 52–64.

[3] B. S. Yeo, S. L. Klaus, P. N. Ross, R. A. Mathies and A. T. Bell, *ChemPhysChem*, 2010, **11**, 1854–1857.

[4] P. A. Giguère and T. K. K. Srinivasan, *J. Raman Spectrosc.*, 1974, **2**, 125–132.

[5] M. Shao, P. Liu and R. R. Adzic, *J. Am. Chem. Soc.*, 2006, **128**, 7408–7409.

[6] C. I. Ratcliffe and D. E. Irish, *Can. J. Chem.*, 1984, **62**, 1134–1144.

[7] T. Itoh, K. Abe, K. Dokko, M. Mohamedi, I. Uchida and A. Kasuya, *J. Electrochem. Soc.*, 2004, **151**, A2042–A2046.

[8] K. M. Ervin, I. Anusiewicz, P. Skurski, J. Simons and W. C. Lineberger, *J. Phys. Chem. A*, 2003, **107**, 8521–8529.

[9] T. M. Ramond, S. J. Blanksby, S. Kato, V. M. Bierbaum, G. E. Davico, R. L. Schwartz, W. C. Lineberger and G. B. Ellison, *J. Phys. Chem. A*, 2002, **106**, 9641–9647.

[10] S. A. Hunter-Saphir and J. A. Creighton, *J. Raman Spectrosc.*, 1998, **29**, 417–419.

[11] J. Kim and A. A. Gewirth, *J. Phys. Chem. B*, 2006, **110**, 2565–2571.

[12] X. Li and A. A. Gewirth, *J. Am. Chem. Soc.*, 2005, **127**, 5252.

[13] J. Brooker, P. A. Christensen, A. Hamnett and R. He, *Faraday Discuss.*, 1992, **94**, 339–360.

[14] M. H. Shao and R. R. Adzic, *J. Phys. Chem. B*, 2005, **109**, 16563–16566.

[15] K. Kunimatsu, T. Yoda, D. A. Tryk, H. Uchida and M. Watanabe, *Phys. Chem. Chem. Phys.*, 2010, **12**, 621–629.

[16] A. Weber and E. A. McGinnis, *J. Mol. Spectrosc.*, 1960, **4**, 195 – 200.

[17] T. Itoh, T. Maeda and A. Kasuya, *Faraday Discuss.*, 2006, **132**, 95–109.